International Journal of Heat and Mass Transfer 97 (2016) 15–25

Contents lists available at ScienceDirect

International Journal of Heat and Mass Transfer

journal homepage: www.elsevier.com/locate/ijhmt

Dropwise gelation-dehydration kinetics during drop-on-demand printing of hydrogel-based materials

Bumsoo Han [a,b,c,*], Gyu Young Yun [a,b], J. William Boley [a,b], Samuel Haidong Kim [d], Jun Young Hwang [d], George T.-C. Chiu [a,b], Kinam Park [b,c]

[a] School of Mechanical Engineering, Purdue University, West Lafayette, IN, USA
[b] Birck Nanotechnology Center, Purdue University, West Lafayette, IN, USA
[c] Weldon School of Biomedical Engineering, Purdue University, West Lafayette, IN, USA
[d] Korea Institute of Industrial Technology, Ansan, Gyeonggi Do, Republic of Korea

ARTICLE INFO

Article history:
Received 27 September 2015
Received in revised form 10 January 2016
Accepted 11 January 2016

Keywords:
Evaporation
Interstitial water transport
Dilatation
Fluid–structure interaction
Consolidation

ABSTRACT

The present study aims to characterize and understand the dropwise gelation-dehydration phenomena during drop-on-demand (DOD) printing of hydrogel-based soft materials. Functional soft materials have broader impacts on many medical and engineering applications, but constructing soft materials into three-dimensional (3D) configuration with spatially varying properties is still extremely challenging. In order to establish a mechanistic understanding, a hypothesis was postulated that the porosity of hydrogel printed is determined by dropwise gelation and dehydration phenomena during the printing process. The underlying rationale is that many functional properties of the printed hydrogels are closely associated with the structural characteristics at the sub-droplet and droplet scales, specifically porosity. The porosity of a hydrogel droplet is thought to be determined by intra-droplet fluid–structure interactions during gelation and dehydration. In this study, thus, we characterized the gelation-dehydration and consequent microstructure of thermally responsive poly(*N*-isopropylacrylamind-*co*-acrylamide) (PNIPAM) copolymer droplets as a model hydrogel material. The gelation kinetics was studied by differential scanning calorimetry. Both macroscopic and microscopic structures of DOD printed hydrogels were characterized by a 3D profiler and scanning electron microscopy. Furthermore, a theoretical model to explain this complex transport processes was also developed. The results showed that the gelation is a rapid process and its impact is mainly observed at the deposition of droplets. Significant structural shrinkage of the printed hydrogel droplets was induced by dehydration. This shrinkage resulted in spatially varying intra-droplet porosity. A computational model of intra-droplet fluid–structure interactions was developed to explain this spatial variation of intra-droplet porosity. In addition, a new dimensionless parameter is proposed to gauge the significance of evaporation and interstitial water transport in the fluid–structure interactions. Significance of gelation kinetics, dehydration and complex fluid–structure interaction within the droplets was discussed to design a DOD printing process for 3D additive manufacturing of hydrogel-based soft materials.

© 2016 Elsevier Ltd. All rights reserved.

1. Introduction

Recent developments of polymer sciences enable numerous novel materials whose properties can be designed and tailored for a wide variety of applications including tissue engineering [1–4], drug delivery [5,6], and energy storage and conversion [7–10]. However, integrating these novel materials into three-dimensional (3D) configurations with spatially varying functional properties is still extremely challenging. For instance, recent developments of biotechnology enable numerous biomaterials which have profound impacts on medicine by providing tissue grafts to replace or treat diseased or damaged tissues [1–4]. Moreover, these biomaterials are also used to develop test beds for drug discovery as well as pathophysiological research [3,11]. In the development of functional biomaterials, 3D physical configuration and organization of cells and tissues are critically important as much as biochemistry. Thus, various methods have been developed to create 3D configurations as reviewed elsewhere [12,13]. However, its capability is still significantly limited, or is very difficult to scale up for rapid fabrication and precise control of their structures at

* Corresponding author at: 585 Purdue Mall, West Lafayette, IN 47906, USA. Tel.: +1 765 494 5626; fax: +1 765 496 7535.
E-mail address: bumsoo@purdue.edu (B. Han).

http://dx.doi.org/10.1016/j.ijheatmasstransfer.2016.01.030
0017-9310/© 2016 Elsevier Ltd. All rights reserved.

multiple length scales. Still most of the fabrication methods have been limited to batch processes. In this context, additive manufacturing of hydrogel-based soft materials has practical significance of enabling new generation functional materials for various applications.

Currently available fabrication methods for additive manufacturing of soft polymeric materials include extrusion based printing [14], laser-assisted polymerization [15], and inkjet based drop-on-demand (DOD) printing [16,17]. Among these methods, DOD printing has the capabilities to create bulk materials with spatially varying functional properties by depositing droplet patterns with desired structural characteristics. Inkjet deposition has been shown in recent studies to be able to deposit a wide range of materials [18]. However, research efforts has been focused on finding reliable jettable conditions, particularly range of viscosity and surface tension, for a given ink material [19–22]. Other approaches are to control jetting parameters to generate droplets at desired volumes [23–25]. This ability created additional degree of freedom to accommodate for the constraints imposed by ink materials. One common drawback of inkjet printing is that the ink material has to be in a liquid phase for injection but should be rapidly polymerized or form gels upon deposition. Additional means are often employed to accelerate the gelation and/or crosslinking such as chemicals, pH, temperature, UV or lasers [26–29]. However, these additional procedures slow down the printing processes and complicate the process control, which is typically established and optimized by repeated experimentations.

Compared to the efforts to identify jettable conditions, behavior of hydrogel ink droplets is rarely studied. Once a small droplet of hydrogel solution is deposited, it will quickly polymerize to form a hydrogel droplet. This droplet will begin to dehydrate at the droplet-air interface due to the evaporation of water. This dehydration will induce droplet shrinkage, which will trigger complex fluid-matrix interactions in the porous hydrogel. These dropwise gelation and dehydration processes are thought to determine droplet scale structure–functionality relationship, which is critically important to realize DOD printing of functional materials with "digitized" (i.e. spatially varying) properties. Although evaporation of solutions and colloidal droplets (i.e., liquid drops where insoluble particles are suspended) have received considerable interests from the research community, understanding this seemingly simple evaporation of droplet is still challenging. The difficulty is caused by the complexity associated with the number of relevant parameters, such as solute concentration, solvent properties, interface characteristics, wettability, and the presence of Marangoni flows [30–33]. Many studies have shown that the ink–substrate interactions determine the evaporation phenomena [31,32,34,35]. One of the most widely recognized features of evaporation of liquid droplets is called the "pinning effect", in which the evaporation occurs in constant contact area mode [36]. The evaporation of a solution droplet with particles makes a ring-shaped structure that is commonly known as "the coffee ring phenomenon". For inkjet printing processes, this patterning process by evaporation can affect the fabrication quality [37].

However, the current understanding on the evaporation of liquid or colloidal droplets is not directly relevant to hydrogel-based soft materials. This is primarily due to the presence of polymer matrix and subsequent fluid–structure interaction at sub-droplet scales. Thus, mechanistic understanding of this complex fluid-matrix interaction during dropwise gelation-dehydration is the critical knowledge gap to be filled to design and develop DOD printing processes for additive manufacturing. Moreover, it will lay the groundwork enabling new generation advanced materials with spatially "digitized" functionality.

In this work, thus, we characterized and analyzed the gelation and dehydration behaviors of hydrogel droplets during DOD printing processes. Specifically, we characterized the gelation-dehydration and consequent microstructure of hydrogel droplets printed on glass substrates. For this study, poly(*N*-isopropylacrylamind-*co*-acrylamide) (PNIPAM) copolymer was used as a model hydrogel material. The PNIPAM was selected because of its thermally responsive gelation kinetics as well as its viscosity suitable for inkjet printing. The present study is based on a hypothesis that complex interaction between polymer matrix and water occurs during this dropwise gelation-dehydration and the result of this interaction will determine the microstructural characteristics of polymers at droplet and sub-droplet scales, specifically porosity of the hydrogel. This structural characteristic is a basic building block of the functional properties of bulk materials fabricated. Furthermore, a theoretical model to explain this complex transport-structure interaction was also developed. The results were further discussed to realize DOD printing for 3D additive manufacturing of hydrogel-based soft materials.

2. Methods

2.1. Preparation of thermally-responsive polymeric ink

For the present study, poly(*N*-isopropylacrylamind-*co*-acrylamide) (PNIPAM) copolymer was used as a model polymer as shown in Fig. 1. This inverse thermopolymer is selected because of its relevance for mechanistic study of the gelation-dehydration phenomena including – (i) its gelation kinetics can be precisely controlled by varying the temperature and polymer concentration, (ii) viscosities and elastic modulus are relevant to DOD printing, and (iii) its chemical inertness makes it suitable to tissue engineering and drug delivery applications. This polymer is in the liquid phase at lower temperatures and forms a gel above its lower critical solution temperature (LCST). Thus, if a polymer solution is prepared below its LCST, it remains in liquid phase, but forms a gel after depositing on a substrate whose temperature is above the gelation temperature. The polymer solution was prepared by dissolving PNIPAM (AO23, Akina PolySciTech, West Lafayette, IN) in 10x PBS at 4 °C with 1%, 2% and 4% (w/v) concentrations. The solution was stored at 4 °C until use.

2.2. Thermal characterization and analysis of gelation kinetics

In order to establish mechanistic understanding of gelation of the polymer solutions during a DOD printing procedure, a thermal analysis of gelation kinetics was performed. By temperature-modulated differential scanning calorimetry (DSC), the gelation temperature and reaction kinetic parameters were characterized by varying the concentration of PNIPAM polymers. Approximately 7–10 μg of each solution was loaded in a sample pan. Then, the pan was hermetically sealed to prevent dehydration during the experiments and was loaded in a differential scanning calorimeter (Q200, TA Instruments, IL) calibrated with indium, water, and sapphire. Measurements were taken during heating from 0 to 40 °C with heating rates of 1, 3 and 5 °C/min. Heat absorption associated

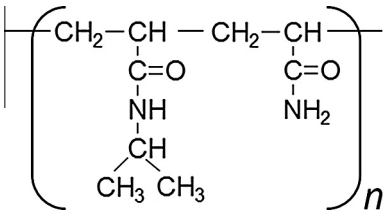

Fig. 1. The chemical structure of inverse thermosentivie poly(*N*-isopropylacrylamind-*co*-acrylamide).

with gelation reaction enthalpy was observed as an endothermic peak in the thermal signal. Based on these results, the gelation process was modeled as a first order reaction. Then, the polymerization fraction, α, was predicted by the Arrhenius reaction model as below:

$$\frac{d\alpha}{dt} = k(1-\alpha) \quad \text{and} \quad k = A \cdot \exp\left[-\frac{\Delta E}{R \cdot T(t)}\right] \tag{1}$$

where k is the reaction constant of the gelation; R is the universal gas constant; and A and ΔE is frequency factor and activation energy of the polymer respectively. The DSC thermograms were curve-fitted to determine A and ΔE, and the polymerization fraction was computed as function of time and temperature.

2.3. Drop-on-demand printing of PNIPAM hydrogel

In order to test the feasibility of hydrogel printing, an inkjet printing platform was constructed as illustrated in Fig. 2. The stationary printhead is an HP Thermal Inkjet Printing System (TIPS) with 12 nozzles with vertical resolution of 400 dot-per-inch (dpi). Although local phase transition might occur near the heater part of the nozzle in the present thermal jet system, the effects of this localized heating are both spatially and temporally negligible on the jetting process. The heating duration was less than 5 μs, and the ink was ejected far from the heating area. Thus, no notable gelation due to thermal jetting process was observed. Substrate movement is provided by an Anorad XY stage with 0.5 μm addressability and maximum linear speed of 30 mm/s. Two video cameras are used to image printed droplets. For printing experiments, the prepared polymer solution was loaded to the ink reservoir of the setup, and the nozzle temperature was maintained in 1–8 °C throughout the experiments. A cold pack was employed to maintain the temperatures of the ink reservoir and nozzle below the gelation temperature of PNIPAM ink. Briefly, an aluminum foil basin was shaped and molded to fit around the ink reservoir and nozzle. The basin was then loaded with an appropriate level of dry ice so that the ink remained in a liquid state. The aluminum foil was then mechanically sealed at the top to enclose the dry ice and reduce large temperature fluctuations. The nozzle temperature was monitored throughout the printing process with a thermocouple embedded in the nozzle. PNIPAM hydrogel droplets were printed in 10×10 pattern on glass substrates in multiple layers. The printing speed was 3 mm/s and the spacing was 300 μm. After the printing, the 3D profiles of droplets printed were assessed by an optical 3D profilometer (Zeta-20, Zeta Instruments, San Jose, CA) with 0.5 μm z-resolution.

At this printing condition, the viscosity and surface tension of 2% w/v PNIPAM ink were characterized. The viscosity was measured using a cone-shape rheometer (AR550, TA instruments). After loading the polymer ink to the rheometer, the viscosity of solution was measured at 0.1 s^{-1} shear strain rate while temperature increased from 2 °C to 8 °C. The viscosity of the polymeric ink at 8 °C was 0.16 ± 0.07 Pa-s ($n = 3$). The surface tension was measured using a standalone force tensiometer (Sigma 702, Biolin Scientific) with a platinum Du Nouy ring. The surface tension of the polymeric ink at 8 °C was 45.2 ± 0.04 mN/m ($n = 5$).

2.4. Scanning electron microscopy

In order to visualize the effects of dropwise gelation-dehydration, the microstructures of the PNIPAM hydrogel matrices were observed by scanning electron microscopy (S-4800, Hitachi) while varying their gelation and dehydration conditions. The polymer solutions were prepared at 4 °C with 1 and 5% w/v concentrations. Then, a small amount of each PNIPAM polymer solution was injected into droplets on a glass substrate at the room temperature and humidity condition (26 °C and 55% relative humidity). After the gelation, the samples were stored at the same temperature but two different controlled relative humidity of 27% and 92%. After 24 h storage, the samples were frozen by being submerged into liquid nitrogen. Then, the frozen samples were freeze-dried for 48 h to remove the imbibed water. The freeze-dried samples were fractured and coated with gold before SEM observation.

2.5. Theoretical analysis of complex transport-structure interactions

A theoretical model was developed to simulate the dehydration of a polymer droplet considering the interactions between polymer matrix and water as illustrated in Fig. 3. Although drying of porous material saturated with water has been studied previously in food sciences and soil mechanics [38–40], dropwise dehydration has not been well studied. In this model, the PNIPAM droplet was approximated to a poroelastic material composed of a porous polymer matrix saturated with water. As the interstitial fluid, i.e., water, evaporates at the droplet-air interface, the polymer matrix will shrink. Due to the constraint at droplet-substrate interface (i.e., constant area dehydration), the droplet will further experience spatially non-uniform deformation. These structural changes result in local change of hydraulic conductivity, and, in turn, will interfere water transport through the matrix. We assumed also that, based on the gelation kinetics study, the gelation would occur rapidly during jetting, and the droplet upon deposition would mainly experience dehydration. The constant area assumption was also validated by photographic observation of the printed droplet (data not shown), which suggested that, for the present ink–substrate, the pinning effect be dominant so that the droplet diameter remained constant during dehydration.

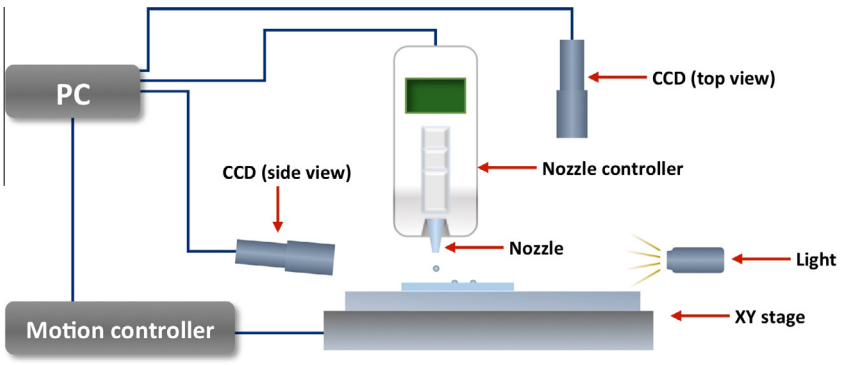

Fig. 2. Schematic of DOD printing setup.

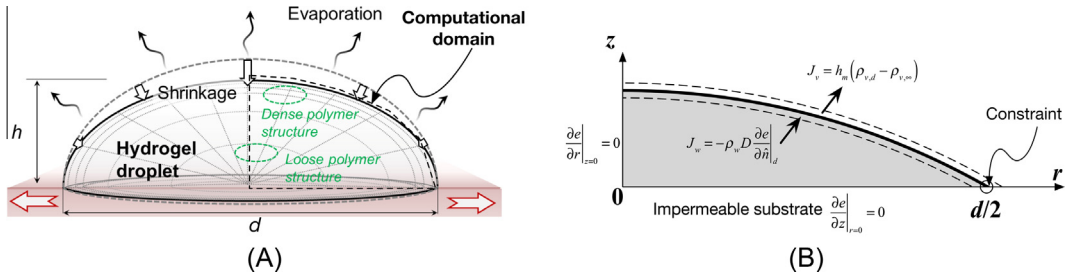

Fig. 3. Schematics of a theoretical model of dropwise dehydration. (A) As a printed droplet is exposed to the ambient, interstitial water in the droplet starts to evaporate at the droplet-air interface. This dehydration results in spatiotemporally varying shrinkage throughout the droplet. Due to the pinning effects, the droplet periphery on the substrate is constrained. This complex fluid–structure interaction is thought to determine the microstructure of the hydrogel droplet. (B) Illustration of the computational domain with corresponding boundary conditions. Because of axisymmetry, the half of the droplet shape was analyzed.

By combining the conservation of mass and momentum for each phase, the local dilatation (i.e., volumetric expansion) of the droplet was modeled by the well-known consolidation equation as below [41–43]:

$$\frac{\partial e}{\partial t} = \nabla \cdot (D \nabla e) \quad \text{and} \quad D = \frac{KE(1-\nu)}{(1+\nu)(1-2\nu)} \tag{2}$$

where e is the dilatation, D is the consolidation constant which is determined by the hydraulic conductivity (K), elastic modulus (E), and Poisson's ratio (ν). If the deformation is small, the dilatation can be related to the local porosity (ϕ) and the initial porosity (ϕ_o) as follows (54):

$$e = \frac{\phi - \phi_o}{1-\phi} \quad \text{or} \quad \phi = \frac{\phi_o + e}{1+e} \tag{3}$$

Since the pore space is saturated with water, the porosity represents the volume fraction of water. Thus, the dilatation is directly correlated to the water content within the droplets. The extent of droplet dehydration was determined by balancing the water evaporation rate, i.e., vapor flux at the droplet-air interface (J_v), with the interstitial water flux (J_w) as illustrated in Fig. 3B:

$$-\rho_w D \left.\frac{\partial e}{\partial \hat{n}}\right|_d = h_m(\rho_{v,d} - \rho_{v,\infty}) \tag{4}$$

where ρ_w is the density of interstitial water, h_m is the mass transfer coefficient at the droplet-air interface, and $\rho_{v,d}$ and $\rho_{v,\infty}$ is the mass concentration of water vapor at the interface and ambient respectively. The mass concentrations are determined from the partial pressure of the vapor (P_v) as follows [44]:

$$\rho_v = \frac{P_v}{1.61P - 0.61P_v} \quad \text{and} \quad P_v = RH \cdot P \tag{5}$$

where P is the total pressure, i.e., ambient pressure, and RH is the relative humidity at a given location. At the droplet-air interface, it is assumed that the vapor is fully saturated so that RH is unity. Since the relative humidity at the ambient during printing experiments was measured at 25–97%, it was assumed at 50% throughout the computations. These equations were solved using a commercial FEM package (COMSOL Multiphysics, Burlington, MA). The properties used in the computation are summarized in Table 1. The ranges of the hydrogel mechanical properties and mass transfer coefficient were selected based on various hydrogel properties in literature [45,46]. In the present computational study, the effects of the ambient humidity change were considered by varying the magnitude of mass transfer coefficient while maintaining the ambient humidity at 50%. Although the evaporation rate is dependent on both mass transfer coefficient and the mass concentration of vapor in the ambient (i.e., ambient humidity), the effects of these two can be consolidated into equivalent mass transfer coefficient at nominal ambient humidity for convenience. The corresponding value of the equivalent mass transfer coefficient is approximately 0.02 m/s for 25% RH, and 0.0008 m/s for 97% RH respectively. Thus, the range of the mass transfer coefficient studied in Table 1 well covers the experimental conditions.

Table 1
Summary of the computational parameters.

Parameters	Values and note
d (diameter of the droplet)	200 μm (mean value from the experiment)
h (height of the droplet)	6 μm (mean value from the experiment)
Contact angle	Approximately 15°
E (elastic modulus)	1000 Pa
K (hydraulic conductivity)	$1 \times 10^{-5} \sim 1 \times 10^{-9}$ m^2/Pa-s
ν (Poisson's ratio)	0.3
h_m (mass transfer coefficient)	0.1, 0.01, 0.001, 0.0001 m/s
ϕ_o (initial porosity)	0.95

3. Results

Fig. 4 summarizes the results of DSC thermal analysis of PNIPAM gelation kinetics. The DSC thermograms confirm the endothermic peaks, which are associated with the gelation process, become sharper with the PNIPAM concentration and the heating rate. The range of the phase transition temperature (i.e., gelation temperature) is within 13–17 °C. The gelation occurs at a lower temperature as the polymer concentration increases. The activation energy (ΔE) of the polymer and the reaction constant (k) of the gelation are computed as summarized in Table 2. The activation energy decreases as the polymer concentration increases. As anticipated, the reaction constant drastically increases with temperature as well as polymer concentration. Thus, as shown in Fig. 4C, the gelation kinetics accelerates as the temperature and polymer concentration increases. For example, at the concentration of 2% and 4% polymer solutions, the complete gelation would occur less than a minute at 15 °C. It is anticipated that the gelation occurs faster during printing as the temperature increases to room temperature. This temperature and concentration dependent gelation kinetics is common properties of thermally-responsive polymers. In a droplet configuration, the gelation is expected to occur even more rapidly considering simultaneous dehydration of polymer solutions during printing, which increases the polymer concentration in the droplet.

The effects of the gelation process are observed on the structure of printed droplets as shown in Fig. 5. In order to demonstrate the feasibility of printing PNIPAM hydrogel in 3D constructs, the droplets were jetted in multiple layers. Macroscopically, the quality of single layer printed droplets was acceptable, which implies that the viscosity and surface tension of the PNIPAM ink are suitable for DOD printing. Microscopically, the single layer droplet clearly

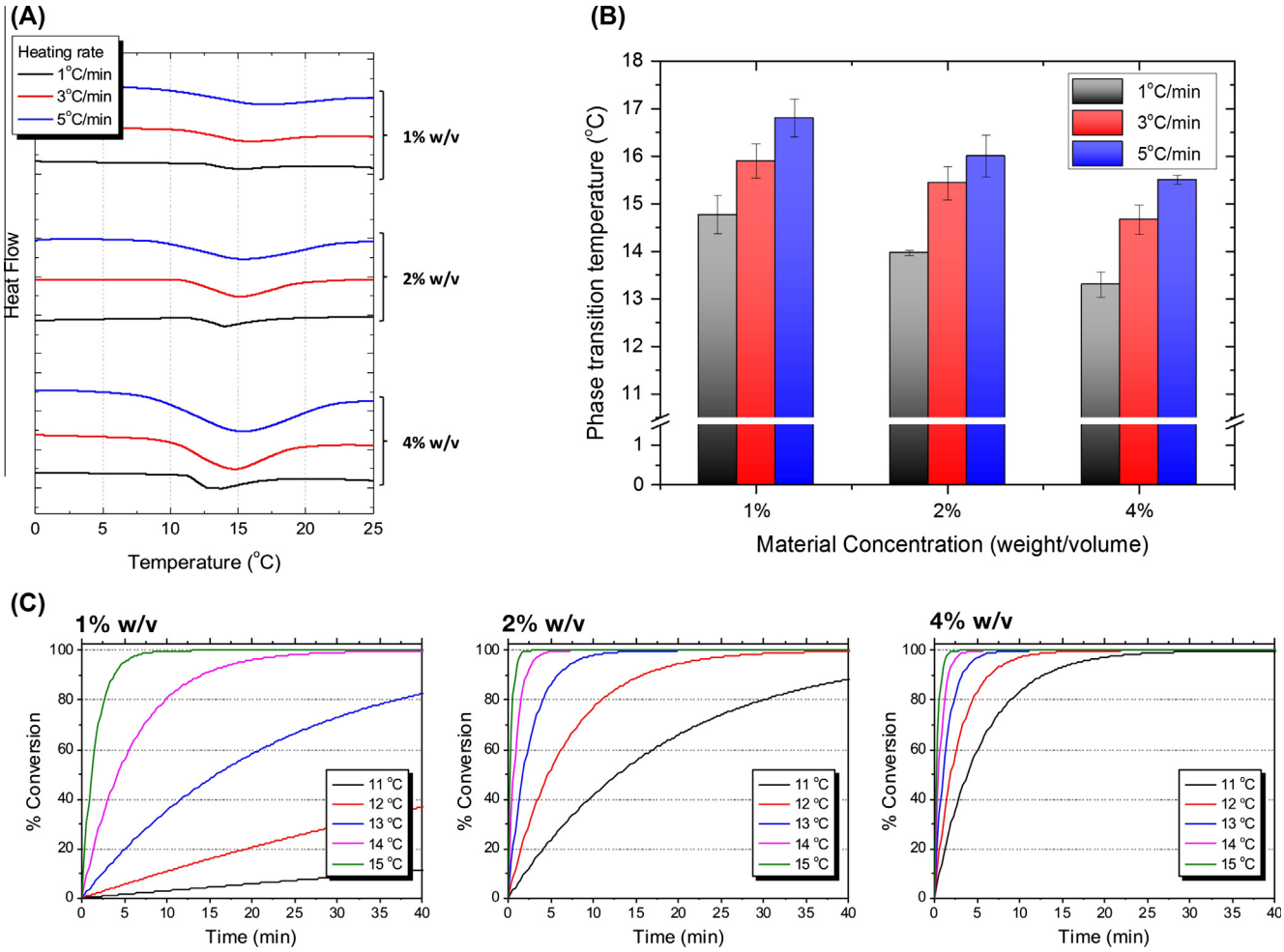

Fig. 4. Thermal analysis of the gelation of PNIPAM polymer solutions. (A) DSC thermograms of PNIPAM while varying the concentration and heating rates. (B) Gelation temperatures. As the concentration increases, the onset of gelation occurs at lower temperature. (C) Isothermal gelation fraction of PNIPAM. This shows the gelation fraction when the polymer is maintained at a given temperature. As the concentration increases and the temperature is elevated, the gelation occurs faster.

Table 2
Thermal analysis of gelation kinetics of PNIPAM.

PNIPAM concentration (% w/v)	Activation energy (ΔE) (kJ/mol)	Reaction constant (k)		
		T = 12 °C	T = 13 °C	T = 14 °C
1	549.34	0.091	0.205	0.458
2	534.90	0.164	0.362	0.793
4	502.44	0.288	0.605	1.263

shows the dehydration with the pinning so that most of ink material is concentrated near the periphery of the droplet. As droplets were printed in multiple layers, however, the quality of printed droplets deteriorated substantially due to a number of secondary droplets. This suggests that, upon depositing (i.e., impacting on the previously printed droplets), the PNIPAM droplet might not be fully polymerized and splashing may occur upon impact. On the contrary, more uniformly distributed ink material is noted during the deposition in multiple layers.

The effects of dehydration on the droplet microstructure are shown in Fig. 6. When the printing occurred at room temperature condition with 55% relative humidity, the evaporation from the droplets occurred during printing. Because of the dehydration, the final droplet profile significantly shrunken so that the maximum height was around 80 μm even after printed in 20 layers (Fig. 6A). Moreover, the top profile of the printed drops was very rough. As shown in Fig. 6B, if the droplets were exposed to high relative humidity (RH = 95%), the droplets swelled back, the maximum height increased to approximately 120 μm and its profile became relatively smooth dome-shaped. The SEM images of the matrix microstructure are also presented. Fig. 6C shows the cross-sectional view of the 1% w/v droplets printed in 92% relative humidity. The porous structure near the droplet-air interface, noted with black arrows, is denser than the interior noted with white arrows. As the humidity decreases (Fig. 6D) or the polymer concentration increases (Fig. 6E), the porous structure become much denser throughout the droplet profiles. This strongly implies the presence of the fluid–structure interaction within the droplets.

The computational results are presented in Fig. 7. Dehydration kinetics of the baseline case ($K = 1 \times 10^{-7}$ m^2/Pa-s, and h_m = 0.01 m/s) is shown in Fig. 7A. As time increases, the dilatation decreases in a spatially non-uniform manner so that high shrinkage is observed near the droplet-air interface. At the periphery of the droplet (i.e., $r = d/2$), significantly higher deformation is localized similar to the "coffee ring effects". This spatially non-uniform deformation may result in spatially non-uniform microstructure of the droplet and eventually generate residual stress in printed products. Since this computed dilatation can be directly converted to the porosity and ultimately water content using Eq. (3), this computational result can provide physical

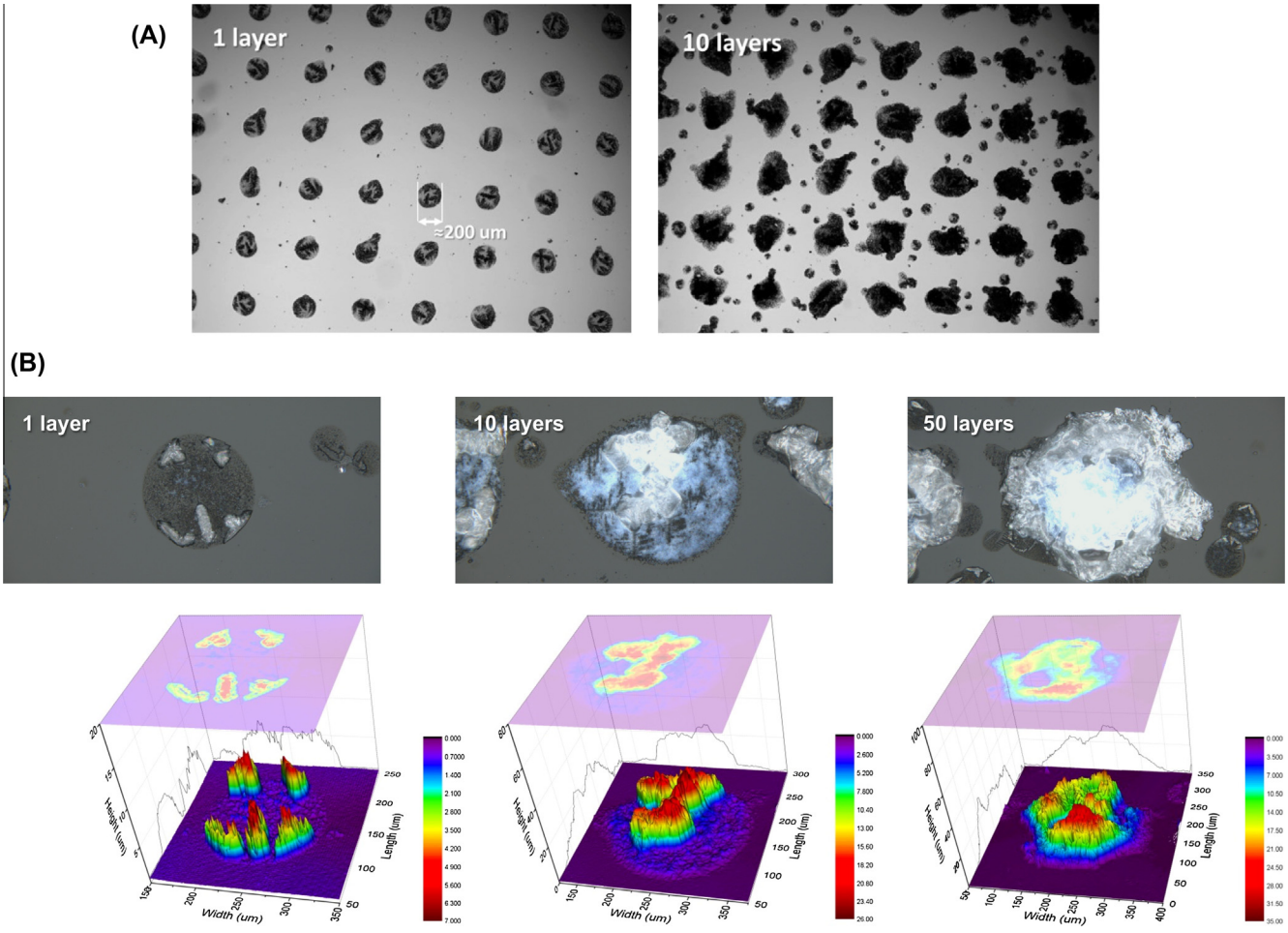

Fig. 5. Droplet structure of PNIPAM polymer solutions printed in multiple layers. (A) Photographs of printed array of droplets. (B) Top panel: Microphotographs of the top views. Bottom panel: 3D profiles of the droplets printed.

insights to interpret the experimental results shown in Fig. 6. For example, the high shrinkage localized near the droplet-air interface matches with the smaller pores near the interface (i.e., black arrows) in Fig. 6C.

The pattern of this intra-droplet deformation is highly dependent on the ink properties and the dehydration conditions, as presented in Fig. 7B. As the hydraulic conductivity increases to 1×10^{-7} m^2/Pa-s (high K case), the deformation occurs throughout the droplet and the magnitude of the maximum dilatation decreases. These changes are thought to be caused by enhanced interstitial water transport. However, as the hydraulic conductivity decreases, the trend reverses and the deformation is highly localized near the droplet-air interface. Interestingly, the magnitude of this highly localized deformation is substantially higher, which can completely shut down interstitial water transport and inhibit the dehydration. This "hydraulic locking" may preserve the water content in the hydrogel, but it may attribute local defects due to significant compaction. The effects of dehydration condition were simulated by varying the mass transfer coefficient. Although the intra-droplet deformation patterns are similar, the magnitude of the maximum dilatation drastically changes. The maximum dilatation of high h_m case is significantly higher than the baseline, which implies significantly decreased pore space. This concurs with experimental observations presented in Fig. 6D, where the droplet experience has significantly smaller pores as the evaporation increases due to low ambient humidity.

4. Discussions

DOD printing of hydrogels has great potential to realize 3D printing of hydrogel-based soft materials, particularly with spatially controlled functional properties. In order to achieve this, mechanistic understanding should be established to correlate among ink properties, printing parameters, and functionality of printed products. Typical DOD printing including the present study consists of three steps – (i) preparation of ink in monomer solution, (ii) printing of the ink into a desired pattern or configuration, and (iii) polymerization and/or dehydration of the polymer droplets to form bulk materials [20,28]. Among these three steps, the last one is most critical for 3D printing since the behaviors of ink droplets during this step, i.e., gelation and concurrent and/or subsequent dehydration, determine the microstructural characteristics of printed products, particularly porosity. Porosity is one of the key structural characteristics of hydrogel-based soft materials. Many functional properties including elastic modulus, hydraulic conductivity, and diffusivity of solutes [47–49] are closely correlated to the porosity. Moreover, the water content is an important characteristic for the functionality of the printed hydrogel. The porosity is also is directly related to the water content of the hydrogel droplets via the volume fraction of interstitial water, since the pore space is assumed to be saturated with water. This assumption is based on our observation that the dehydration is a slow process and can be approximated to a quasi-equilibrium process. During

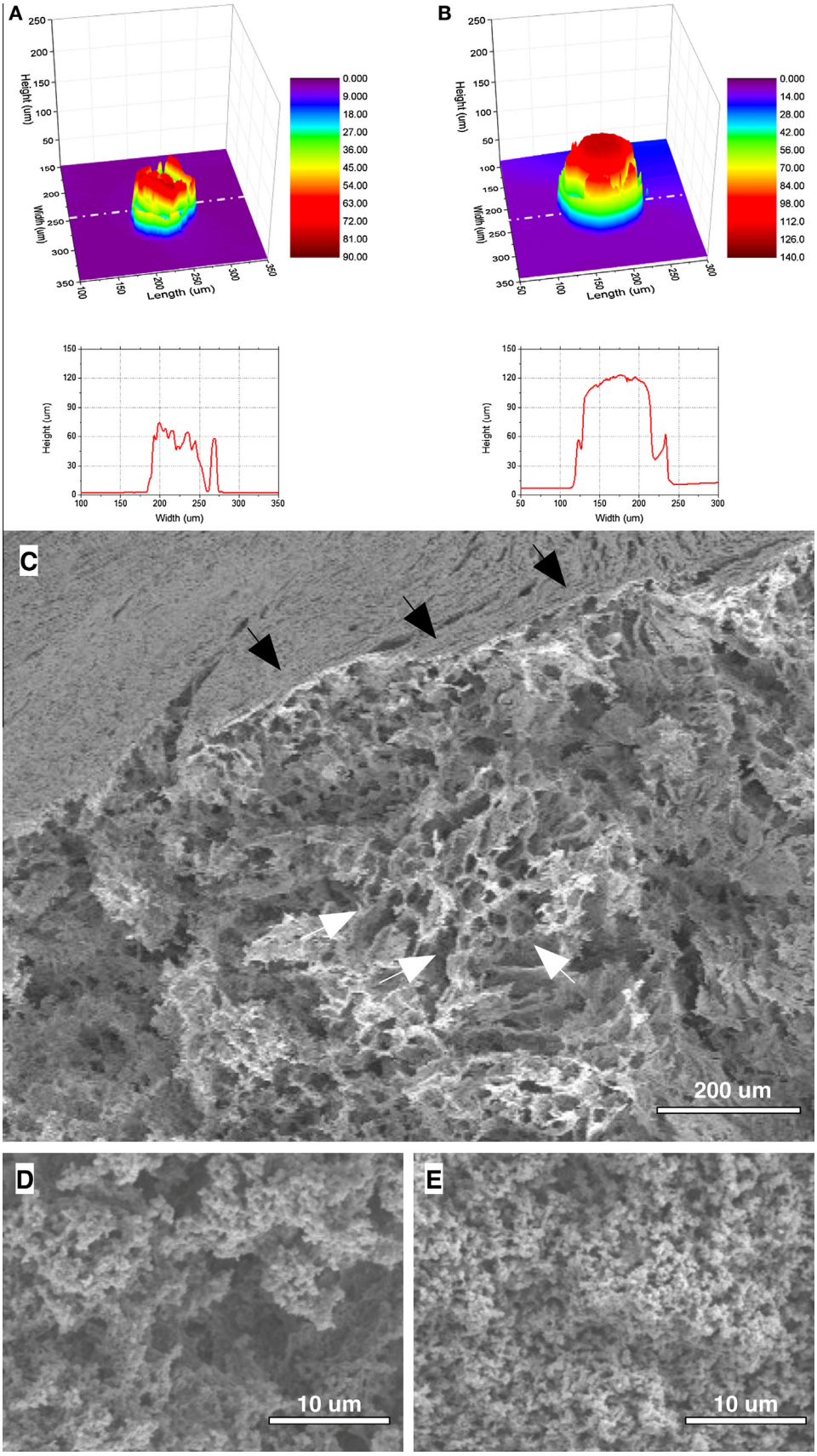

Fig. 6. Effects of dehydration on the droplet microstructures. (A) 3D profile of a droplet printed at 55% relative humidity. (B) 3D profile of a droplet exposed to 95% relative humidity. (C–E) SEM images of the internal microstructures of PNIPAM hydrogel droplets: 1% w/v PNIPAM at 92% RH (C), 1% w/v at 27% RH (D), and 5% w/v at 27% RH (E).

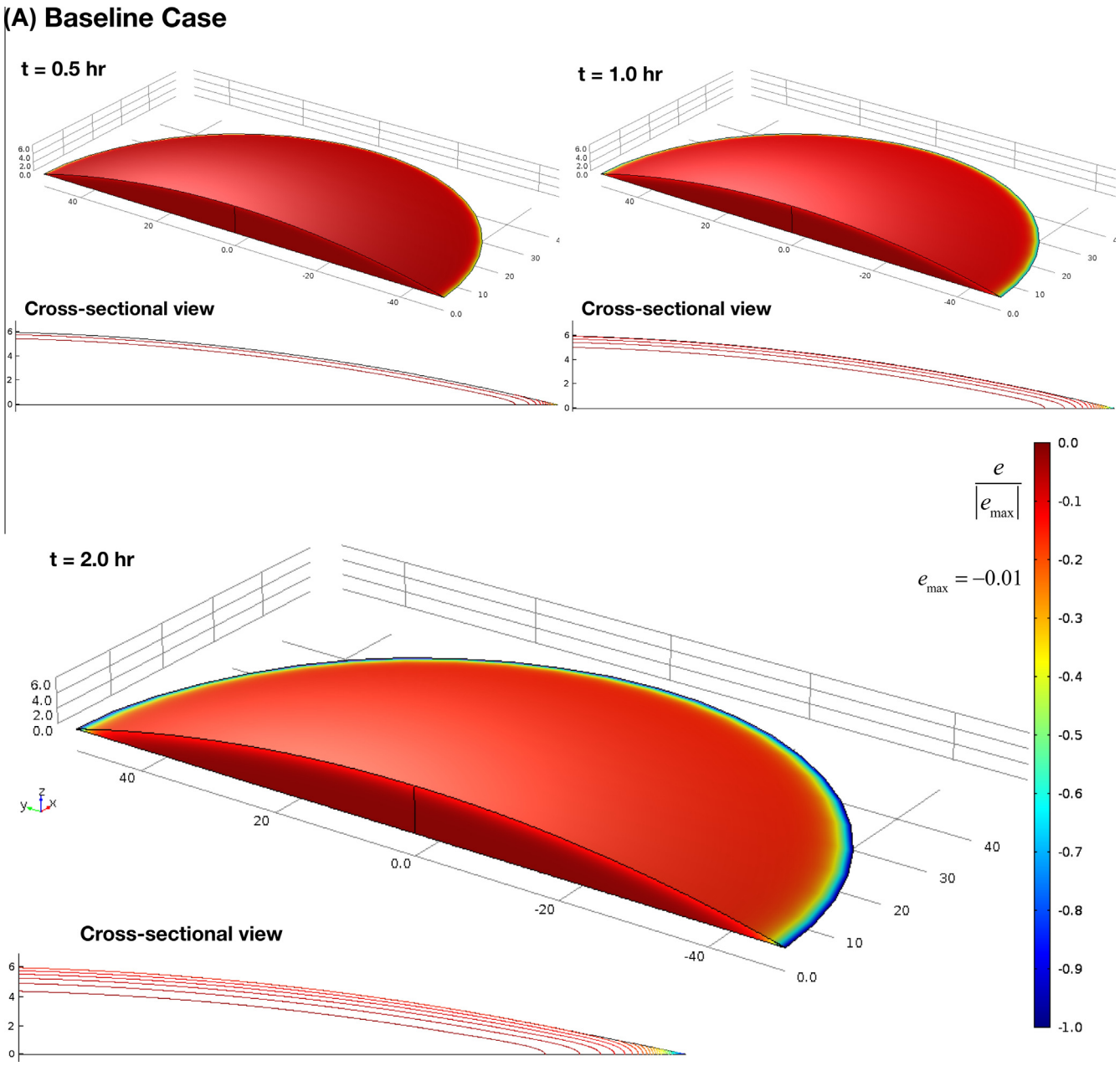

Fig. 7. Computational prediction of intradroplet deformation of PNIPAM hydrogel droplets during dehydration. (A) Time-lapse contour of dilatation during dropwise dehydration of hydrogel with baseline properties ($K = 1 \times 10^{-7}$ m^2/Pa-s, and $h_m = 0.01$ m/s). (B) Effects of hydraulic conductivity ($K = 1 \times 10^{-5}$ m^2/Pa-s or 1×10^{-9} m^2/Pa-s) and mass transfer coefficient ($h_m = 0.1$ m/s or $h_m = 0.0001$ m/s) on the dilatation of hydrogel droplets after 2 h dehydration. All the color contours are plotted along the color scale of $e/|e_{max}|$ shown in (A). Cross-sectional dilatation contours are plotted at the interval of $e/|e_{max}| = -0.05$ (For interpretation of the references to color in this figure legend, the reader is referred to the web version of this article.).

dehydration, thus, the behavior of the hydrogel droplets could be approximated to a poroelastic material whose interstitial space (i.e., pores) is saturated with water. As the water evaporates at the droplet-air interface, the interstitial water at the interior of the droplet transports toward the interface across the dilatation gradient described in Eq. (2). As a result, the droplet shrinks and its porosity (i.e., water content) decreases. Thus, precise control of the porosity will enable advanced materials with "digitized" functional properties for various applications including tissue engineering, drug delivery, printed electronics, and energy applications.

In order to properly control the porosity, dynamics of three transient processes should be understood – (i) gelation, (ii) dehydration, and (iii) jetting. The interplay among these processes will significantly affect the microscopic porosity within the droplet as well as drop-drop interfaces as illustrated in Fig. 8. For the PNIPAM polymer studied, the gelation is a rapid reaction, but it will affect the deposition process. After deposition of a small droplet of polymer solution (20–100 pl) on an impermeable substrate, the polymer solution may undergo rapid dropwise gelation whose kinetics is dependent on the temperature and concentration of the polymer. Because of small volume and rapid reaction, it is expected to quickly polymerize and form a hydrogel droplet.

As the hydrogel droplet forms, water in the droplet evaporates across its top surface. As a result of this evaporation, the droplet shrinks and the polymer matrix near the droplet-air interface

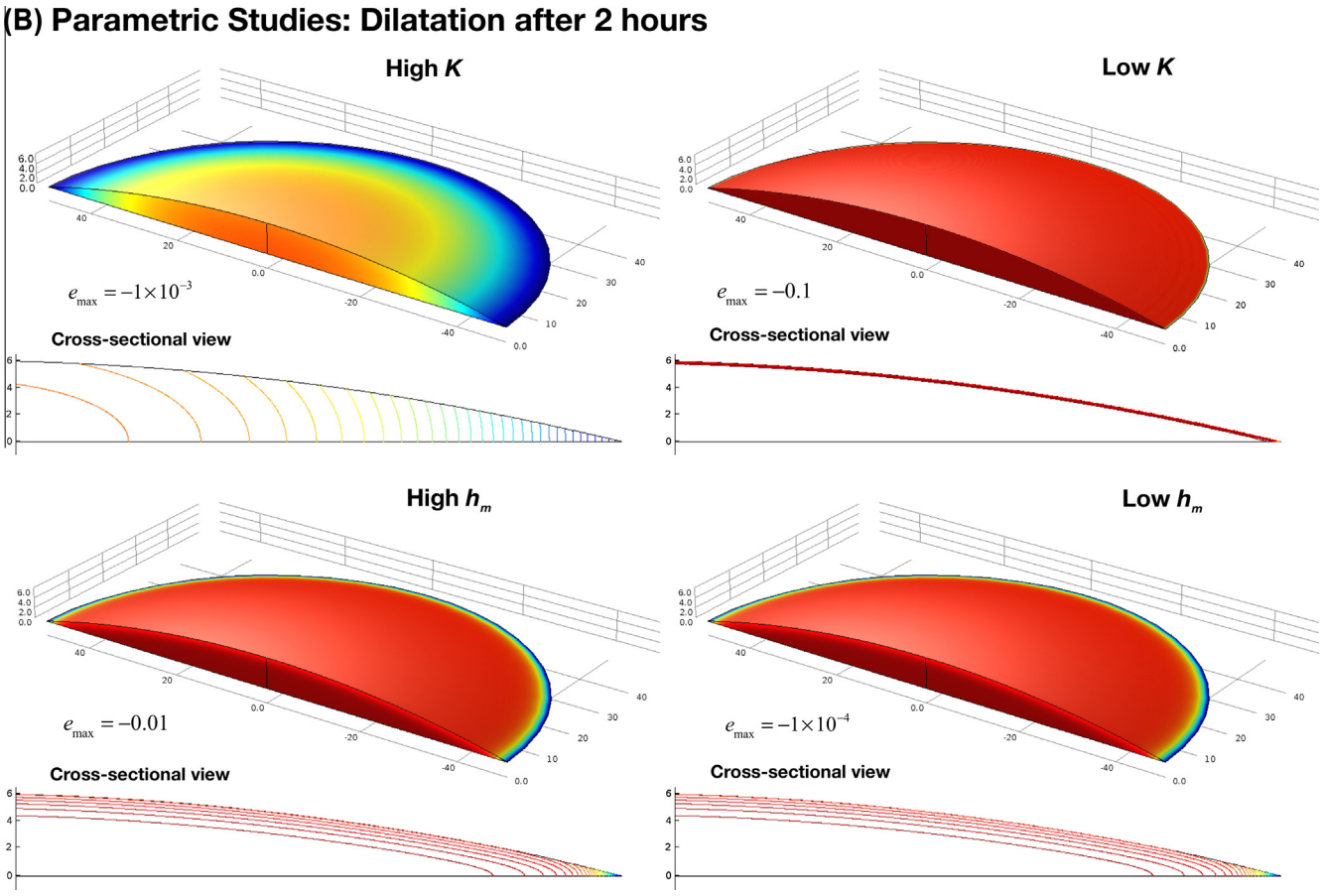

Fig. 7 (*continued*)

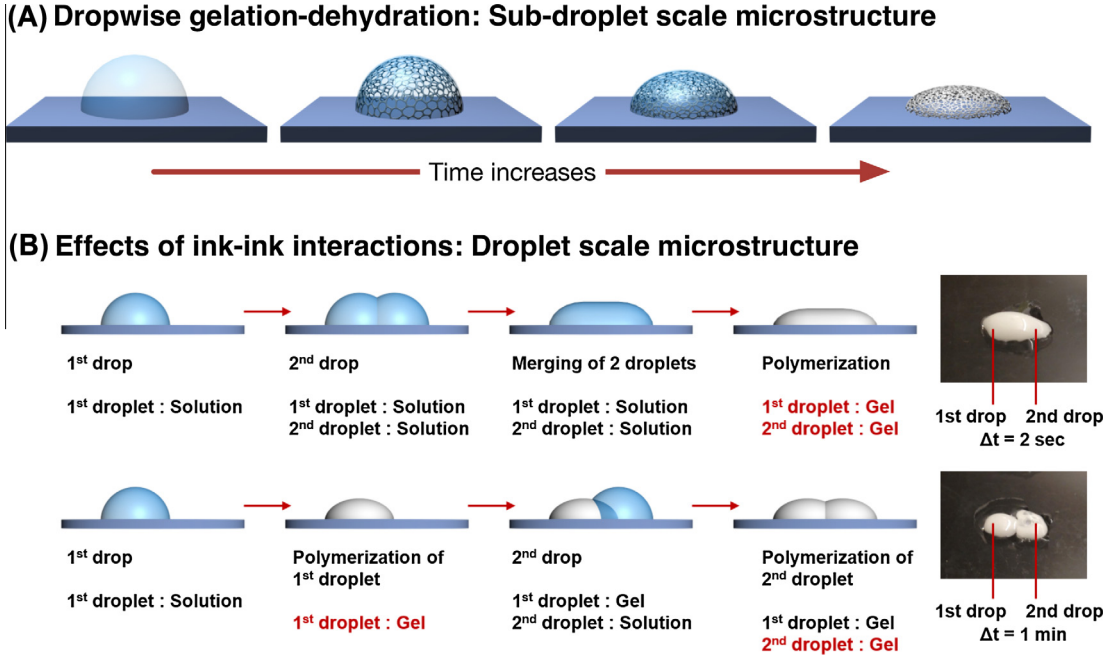

Fig. 8. Schematic illustration of the sub-droplet and droplet scale microstructures during DOD printing of hydrogel-based ink. (A) After deposited on an impermeable substrate, a droplet of the hydrogel polymer solution undergoes gelation and porous polymer matrix is formed. As evaporation occurs at the droplet-air interface, the droplet is dehydrated and its matrix structure shrinks. This deformation decreases the local hydraulic conductivity of the matrix and subsequent water transport within the droplet. The result of this interaction determines the final microstructure, i.e., porosity. (B) The time scale of printing and gelation will also affect droplet scale microstructure via two different ink–ink interaction scenarios – (top) when time scale of printing is shorter than that of gelation, two ink droplets will coalesce and form one large droplet. (bottom) If the time scale of printing is longer than gelation, the gelation of the 2nd drop will be affected by water transport between these top droplets. The resulting microstructure is distinctly different from the prior scenario.

Table 3
Dimensionless parameter of the computational cases studied.

Computational cases	Mass transfer coefficient (h_m) (m/s)	Hydraulic conductivity (K) (m^2/Pa-s)	Consolidation constant (D) (m^2/s)	Dimensionless parameter ($h_m L_c/D$)
Baseline	0.01	1×10^{-7}	1.4×10^{-4}	4.5×10^{-4}
High K	0.01	1×10^{-5}	1.4×10^{-2}	4.5×10^{-6}
Low K	0.01	1×10^{-9}	1.4×10^{-6}	4.5×10^{-2}
High h_m	0.1	1×10^{-7}	1.4×10^{-4}	4.5×10^{-3}
Low h_m	0.0001	1×10^{-7}	1.4×10^{-4}	4.5×10^{-6}

becomes denser than the interior of the droplet. As the matrix become denser, the local hydraulic conductivity decrease which reciprocally impedes the intra-droplet water transport. The extent of this fluid-matrix interaction is dependent on the properties of the hydrogel materials, and is further complicated by constraints at ink–substrate interface. As mentioned previously [31,32], depending on the wettability and mode of dehydration, the substrate may constrain the droplet shrinkage, and affect the local matrix deformation and subsequent water transport. Thus, the modes of evaporation – constant contact angle or constant contact area, will also affect the final printed patterns in addition to the gelation kinetics. For the present ink–substrate configuration, PNIPAM hydrogel on glass substrate, evaporation occurred in constant contact area mode.

The key mass transfer process of this dropwise dehydration is determined by the mass conservation at the drop-air interface as described in Eq. (4). By performing scaling analysis, a relevant dimensionless parameter can be formulated to explain the significance of this dehydration process as below.

$$\rho_w D \frac{\Delta e}{L_c} \sim h_m \Delta \rho_v \;\rightarrow\; \frac{h_m L_c}{D} \sim \frac{[Evaporation]}{[Interstitial\ water\ transport]} \tag{6}$$

This Nusselt number-like parameter represents the significance of evaporation with respect to interstitial water transport, which is mathematically expressed as the diffusion of dilatation in Eq. (2). The consolidation constant (D) relates to two key mechanical properties of the hydrogel materials – hydraulic conductivity (K) and elastic modulus (E). The values of the proposed parameter are summarized in Table 3 for the computational cases shown in Fig. 7. These values are computed with the droplet height the characteristic length, since the dehydration and subsequent interstitial water transport mainly occurred along the z-axis. As the mass transfer coefficient (h_m) increases or the consolidation constant (D) decreases, the parameter will increase which suggests that the evaporation become dominant. Thus, compared to the baseline case, the droplets in these two cases are expected have smaller pores and condensed matrix structure. On the contrary, as h_m decreases and D decreases, the parameter implies that the interstitial water transport occurs rapidly so that the droplets will experience less deformation gradient and spatially uniform matrix microstructure for a given evaporation rate. Although further research is warranted, this parameter can be a predictive measure of the quality of the printed droplet. It may also provide a quantitative guideline to adjust printing parameters and ink properties to achieve the same microstructural characteristics of new ink materials.

As printing occurs in multiple layers, the ink–ink interaction will add additional complexities to the dropwise gelation-dehydration phenomena. After deposition on or near another layer of printed hydrogel droplets, the newly printed hydrogel droplet will undergo dehydration process including complex matrix-fluid interactions with the other droplets as illustrated in Fig. 8B. In addition to these, the shrinkage of the droplet also induces the deformation of the polymer substrate, whose magnitude should depend on the elastic modulus of the polymer substrate. Moreover, due to the substrate deformation and imbalance of the elastic stress of the polymer matrix in the intra-droplet space and the substrate, additional water transport is expected to occur at the droplet-substrate (i.e., ink–ink) interfaces, which is absent in the ink–substrate interaction.

If a printing process is performed at a humid environment, the dehydration may be minimized. However, the evaporation cannot be completely avoided. It is much more desirable to print at the ambient condition for convenience and maintenance of the processes and equipment. Often, high water content is desired to matching jettable viscosity and surface tension. Thus, the significance of dehydration during DOD printing cannot be overemphasized. This will also mitigate the material selectively of DOD printing, and enable broader manufacturing of hydrogel-based materials. Although the mechanistic explanation proposed in the present study may be able to explain the dropwise gelation-dehydration with fluid–structure interactions, it should be validated with other types of polymers whose gelation and structural properties varies. It also needs to be further developed considering fluid–structure interactions at ink–ink interfaces during 3D printing. Although the results from the present study may provide mechanistic explanation of the final porosity of printed hydrogel droplets, further research is still warranted to measure the changes of water content such as using thermogravimetric analyzer or differential scanning calorimeter. However, this is very difficult because the amount of printed droplets is too small to obtain measurable weight difference or because the thermal signature is affected by the reversible gelation kinetics of PNIPAM. Moreover, the computational model also assumed constant properties during dehydration. However, these properties are closely related to the matrix porosity, which varies notably during the dehydration process. Further development incorporating deformation dependent properties may also be necessary.

5. Conclusions

In the present study, droplet and sub-droplet scale fluid–structure interactions have been both experimentally and computationally studied to predict DOD printed droplet's porosity considering dropwise gelation-dehydration. Sub-droplet level fluid–structure interaction is proposed as an underlying mechanism to determine the final porosity. It is demonstrated that sub-droplet scale fluid-matrix interactions should be correlated to polymer gelation kinetics, dehydration as well as printing process parameters such as spatial and temporal deposition parameters between adjacent drops (when and where adjacent drops should be deposited and the associated structural–functionality) and between layers. The results will be useful to lay the groundwork to enable new generation materials with desired functionalities via DOD printing.

Acknowledgements

This study is partially supported by an International Collaboration grant from Korea Institute of Industrial Technology, and by Brian Pool Program by the Korean Federation of Science

and Technology Societies. The authors would like to acknowledge the generous support of Hewlett-Packard company for using the HP Researcher's Inkjet Development Kit (TIPS).

References

[1] J.L. Drury, D.J. Mooney, Hydrogels for tissue engineering: scaffold design variables and applications, Biomaterials 24 (24) (2003) 4337–4351.
[2] L.A. Hockaday, K.H. Kang, N.W. Colangelo, P.Y.C. Cheung, B. Duan, E. Malone, J. Wu, L.N. Girardi, L.J. Bonassar, H. Lipson, C.C. Chu, J.T. Butcher, Rapid 3D printing of anatomically accurate and mechanically heterogeneous aortic valve hydrogel scaffolds, Biofabrication 4 (3) (2012).
[3] H. Yoshida, M. Matsusaki, M. Akashi, Multilayered blood capillary analogs in biodegradable hydrogels for in vitro drug permeability assays, Adv. Funct. Mater. 23 (14) (2013) 1736–1742.
[4] Y. Zhao, R. Yao, L. Ouyang, H. Ding, T. Zhang, K. Zhang, S. Cheng, W. Sun, Three-dimensional printing of Hela cells for cervical tumor model in vitro, Biofabrication 6 (3) (2014).
[5] Y. Qiu, K. Park, Environment-sensitive hydrogels for drug delivery, Adv. Drug Deliv. Rev. 64 (Supplement) (2012) 49–60.
[6] L.A. Sharpe, A.M. Daily, S.D. Horava, N.A. Peppas, Therapeutic applications of hydrogels in oral drug delivery, Exp. Opin. Drug Deliv. 11 (6) (2014) 901–915.
[7] J. Fawaz, K. Wang, A. Almansoori, Energy gas storage in porous polymers, in: V. Mittal (Ed.), Polymers for Energy Storage and Conversion, John Wiley & Sons Inc, 2013, pp. 215–248.
[8] J. Hur, K. Im, S. Hwang, B. Choi, S. Kim, S. Hwang, N. Park, K. Kim, DNA hydrogel-based supercapacitors operating in physiological fluids, Sci. Rep. 3 (2013).
[9] L. Pan, G. Yu, D. Zhai, H.R. Lee, W. Zhao, N. Liu, H. Wang, B.C.K. Tee, Y. Shi, Y. Cui, Z. Bao, Hierarchical nanostructured conducting polymer hydrogel with high electrochemical activity, PNAS 109 (24) (2012) 9287–9292.
[10] Y. Sahai, J. Ma, High performance polymer hydrogel based materials for fuel cells, in: V. Mittal (Ed.), Polymers for Energy Storage and Conversion, John Wiley & Sons Inc, 2013, pp. 1–25.
[11] R. Kostadinova, F. Boess, D. Applegate, L. Suter, T. Weiser, T. Singer, B. Naughton, A. Roth, A long-term three dimensional liver co-culture system for improved prediction of clinically relevant drug-induced hepatotoxicity, Toxicol. Appl. Pharmacol. 268 (1) (2013) 1–16.
[12] P. Bajaj, R.M. Schweller, A. Khademhosseini, J.L. West, R. Bashir, 3D biofabrication strategies for tissue engineering and regenerative medicine, Annu. Rev. Biomed. Eng. 16 (1) (2014) 247–276.
[13] S.V. Murphy, A. Atala, 3D bioprinting of tissues and organs, Nat. Biotechnol. 32 (8) (2014) 773–785.
[14] C. Norotte, F. Marga, L. Niklason, G. Forgacs, Scaffold-free vascular tissue engineering using bioprinting, Biomaterials 30 (30) (2009) 5910–5917.
[15] R.A. Barry, R.F. Shepherd, J.N. Hanson, R.G. Nuzzo, P. Wiltzius, J.A. Lewis, Direct-write assembly of 3D hydrogel scaffolds for guided cell growth, Adv. Mater. 21 (23) (2009) 2407–2410.
[16] K. Jakab, C. Norotte, F. Marga, K. Murphy, G. Vunjak-Novakovic, G. Forgacs, Tissue engineering by self-assembly and bio-printing of living cells, Biofabrication 2 (2) (2010).
[17] G. Villar, A.D. Graham, H. Bayley, A tissue-like printed material, Science 340 (6128) (2013) 48–52.
[18] J.R. Castrejon-Pita, W. Baxter, J. Morgan, S. Temple, G. Martin, I. Hutchings, Future, opportunities and challenges of inkjet technologies, Atomization Sprays 23 (6) (2013) 541–565.
[19] A.U. Chen, O.A. Basaran, A new method for significantly reducing drop radius without reducing nozzle radius in drop-on-demand drop production, Phys. Fluids 14 (2002).
[20] B. Derby, Inkjet printing of functional and structural materials: fluid property requirements, feature stability, and resolution, Annu. Rev. Mater. Res. 40 (2010) 395–414.
[21] S. Fathi, P. Dickens, R. Hague, Jetting stability of molten caprolactam in an additive inkjet manufacturing process, Int. J. Adv. Manuf. Technol. 59 (1–4) (2012) 201–212.
[22] E. Kim, J. Baek, Numerical study on the effects of non-dimensional parameters on drop-on-demand droplet formation dynamics and printability range in the up- scaled model, Phys. Fluids 24 (2012).
[23] A.A. Castrejón-Pita, J.R. Castrejón-Pita, G.D. Martin, A novel method to produce small droplets from large nozzles, Rev. Sci. Instrum. 83 (2013).
[24] J.R. Castrejón-Pita, N.F. Morrison, O.G. Harlen, G.D. Martin, I.M. Hutchings, Experiments and Lagrangian simulations on the formation of droplets in drop-on-demand mode, Phys. Rev. E 83 (2011).
[25] A. Fulton, J.W. Boley, N. Bajaj, G.T.C. Chiu, T.S. Fisher, A novel method for stable control of drop volume with constant nozzle radius in thermal inkjet systems, in: Proceedings of the NIP30 the International Conference on Digital Printing Technologies and Digital Fabrication 2014, 2014.
[26] W.E. Hennink, C.F. van Nostrum, Novel crosslinking methods to design hydrogels, Adv. Drug Deliv. Rev. 54 (1) (2002) 13–36.
[27] S. Khalil, W. Sun, Biopolymer deposition for freeform fabrication of hydrogel tissue constructs, Mater. Sci. Eng., C 27 (3) (2007) 469–478.
[28] S.V. Murphy, A. Skardal, A. Atala, Evaluation of hydrogels for bio-printing applications, J. Biomed. Mater. Res. 101A (1) (2013) 272–284.
[29] A. Skardal, J. Zhang, G.D. Prestwich, Bioprinting vessel-like constructs using hyaluronan hydrogels crosslinked with tetrahedral polyethylene glycol tetracrylates, Biomaterials 31 (24) (2010) 6173–6181.
[30] T.A.H. Nguyen, A.V. Nguyen, Increased evaporation kinetics of sessile droplets by using nanoparticles, Langmuir 28 (49) (2012) 16725–16728.
[31] Z. Pan, J.A. Weibel, S.V. Garimella, Influence of surface wettability on transport mechanisms governing water droplet evaporation, Langmuir 30 (32) (2014) 9726–9730.
[32] D.H. Shin, S.H. Lee, J.-Y. Jung, J.Y. Yoo, Evaporating characteristics of sessile droplet on hydrophobic and hydrophilic surfaces, Microelectron. Eng. 86 (4–6) (2009) 1350–1353.
[33] B.M. Weon, J.H. Je, Coalescence preference depends on size inequality, Phys. Rev. Lett. 108 (22) (2012).
[34] C. Bourgès-Monnier, M.E.R. Shanahan, Influence of evaporation on contact angle, Langmuir 11 (7) (1995) 2820–2829.
[35] S.M. Rowan, M.I. Newton, G. McHale, Evaporation of microdroplets and the wetting of solid-surfaces, J. Phys. Chem. 99 (35) (1995) 13268–13271.
[36] R.D. Deegan, O. Bakajin, T.F. Dupont, G. Huber, S.R. Nagel, T.A. Witten, Capillary flow as the cause of ring stains from dried liquid drops, Nature 389 (October) (1997) 827–829.
[37] D. Soltman, V. Subramanian, Inkjet-printed line morphologies and temperature control of the coffee ring effect, Langmuir 24 (5) (2008) 2224–2231.
[38] P. Perré, I.W. Turner, A 3-D version of TransPore: a comprehensive heat and mass transfer computational model for simulating the drying of porous media, Int. J. Heat Mass Transfer 42 (24) (1999) 4501–4521.
[39] K. Khalfaoui, S. Chemkhi, F. Zagrouba, Modeling and stress analysis during drying of a deformable and saturated porous medium, Drying Technol. Int. J. 31 (2013) 1124–1137.
[40] B. Jankovic, B. Adnadevic, J. Jovanovic, Application of model-fitting and model-free kinetics to the study of non-isothermal dehydration of equilibrium swollen poly (acrylic acid) hydrogel: thermogravimetric analysis, Thermochim. Acta 452 (2007) 106–115.
[41] B. Han, J.D. Miller, J.K. Jung, Freezing-induced fluid-matrix interaction in poroelastic material, J. Biomech. Eng. 131 (2009).
[42] K.Y. Teo, T.O. DeHoyos, J.C. Dutton, F. Grinnell, B. Han, Effects of freezing-induced cell-fluid-matrix interactions on the cells and extracellular matrix of engineered tissues, Biomaterials 32 (2011) 5380–5390.
[43] A. Ozcelikkale, B. Han, Nanoscale fluid-structure interactions in cytoplasm during freezing, in: Proceedings of the ASME 2012 International Mechanical Engineering Congress & Exposition, IMECE2012-88161, 2012.
[44] W.M. Kays, M.E. Crawford, Convective Heat and Mass Transfer, McGraw Hill, 1993.
[45] S. Park, C. Whittington, S.L. Voytik-harbin, B. Han, Microstructural parameter-based modeling for transport properties of collagen matrices, J. Biomech. Eng. 137 (061003) (2015) 061001–061009.
[46] S. Park, A. Seawright, S. Park, J. Craig Dutton, F. Grinnell, B. Han, Preservation of tissue microstructure and functionality during freezing by modulation of cytoskeletal structure, J. Mech. Behav. Biomed. Mater. 45 (2015) 32–44.
[47] W.Y. Gu, H. Yao, A.L. Vega, D. Flagler, Diffusivity of ions in agarose gels and intervertebral disc: effect of porosity, Ann. Biomed. Eng. 32 (2004) 1710–1717.
[48] E.M. Johnson, W.M. Deen, Hydraulic permeability of agarose gels, AIChE J. 42 (1996) 1220–1224.
[49] J.A. White, W.M. Deen, Agarose-Dextran gels as synthetic analogs of glomerular basement membrane: water permeability, Biophys. J . 82 (2002) 2081–2089.